Available online at www.sciencedirect.com

ScienceDirect

Procedia Engineering 102 (2015) 190 – 200

Procedia Engineering

www.elsevier.com/locate/procedia

The 7th World Congress on Particle Technology (WCPT7)

In situ Raman monitoring of the formation and growth of carbon nanotubes via chemical vapor deposition

Karla Reinhold-López[a,b], Andreas Braeuer[a,b], Bettina Romann[a], Nadejda Popovska-Leipertz[c,d] and Alfred Leipertz[a,b,d,*]

[a]*Lehrstuhl für Technische Thermodynamik, Friedrich-Alexander Universität Erlangen-Nürnberg, Erlangen, Germany*

[b]*Erlangen Graduate School in Advanced Optical Technologies (SAOT), Friedrich-Alexander Universität Erlangen-Nürnberg,, Germany*

[c]*Lehrstuhl für Chemische Reaktionstechnik, Friedrich-Alexander Universität Erlangen-Nürnberg, Erlangen, Germany*

[d] *ESYTEC, Energie- und Systemtechnik GmbH, Erlangen, Germany*

Abstract

An *in situ* measurement technique based on Raman spectroscopy is established to simultaneously monitor the parameters of interest of the solid and gas phases during the formation and growth of carbon nanotubes (CNT) in a cold wall reactor for catalytic chemical vapor deposition (CCVD). Iron nanoparticles were used as a catalyst and acetylene as a carbon source. This new developed technique makes possible the simultaneous *in situ* measurement of the gas phase composition, the gas phase temperature and the micro structure of the deposited CNTs, such that finally the decomposition of the carbon source and its effect on the gas temperature and on the CNTs formation and growth can be followed as a function of the reaction time. Comprehensive qualitative and quantitative analyses have been performed to assess the catalyst performance with respect to the growing carbon nanostructures. On the basis of the real-time *in situ* Raman spectra of the emerging solid phase, the moment of nucleation or first signal detection, the time-range of the CNT growth and the end of the deposition is monitored via the characteristic D and G Raman bands for carbon materials. Information about catalytic activity is qualitatively provided and the estimated *in situ* D/G ratio reveals the defect and disorder content of the growing nanostructures. The Raman spectroscopy setup for the gas phase analysis exhibits high detection sensitivity as well as high accuracy and precision. Correlation could be found between the catalyst activity, acetylene conversion and micro structure of the resulting CNTs.

Selection and peer-review under responsibility of Chinese Society of Particuology, Institute of Process Engineering, Chinese Academy of Sciences (CAS)

* Corresponding author. Tel +49 1714949857, Fax +49 9131 898451, alfred.leipertz@fau.de

Selection and peer-review under responsibility of Chinese Society of Particuology, Institute of Process Engineering, Chinese Academy of Sciences (CAS)
doi:10.1016/j.proeng.2015.01.126

Keywords: carbon nanotubes; catalytic chemical vapor deposition, Raman spectroscopy, in situ monitoring

1. Introduction

Carbon nanotubes (CNTs) have drawn the attention of researchers in a wide range of fields, not only because of their unique properties compared to conventional materials but also because of their very promising potential applications in future technologies. However, the extensive use of this material requires the development of scalable and selective formation processes; among them the catalytic chemical vapor deposition (CCVD) process is considered to be the most promising because of its simplicity, its low cost and the possibility of industrial scale-up due to the relatively low growth temperatures, high yields and high purities that can be achieved [1].

The CCVD process involves feeding a volatile precursor into a reactor containing a heated substrate. Typically, transition metal nanoparticles are used to catalyze the thermal decomposition of the precursor leading to CNT formation and growth [2]. Chemical reactions occur in the gas phase and on the heated substrate and are accompanied by the production of exhaust by-products that leave the reactor together with residual reaction gases. Even though the CNT formation and growth mechanisms by CCVD have been extensively studied in the past using theoretical models and simulations [3-5], there is still no general agreement about what the actual influence of the input parameters on the resulting structures is, so that the process can be optimized towards a CNT tailor-made production. The intermediate processes taking place inside the reactor, such as gas flow dynamics and chemical reactions in the gas phase as well as the formation and growth mechanisms in the solid phase (CNTs) should be analyzed as a whole and thus, not only limit to the analysis of input and output data in experimental studies. To date, Raman spectroscopy has been extensively used for the structural *ex situ* characterization of carbon-based materials as well as for studying their basic properties, mainly owing to its richness in information content. In addition, this technique is also suitable for *in situ* non-invasive measurements at gaseous molecules, as it enables the determination of their temperature and composition with high precision and accuracy. On this account, our approach is focused on implementing this powerful measurement technique to monitor *in situ* the CNT deposition. First, we have reported our measurement strategy to monitor *in situ* the gas phase temperature and the carbon source conversion by applying Raman spectroscopy near the substrate at CCVD operation conditions but without using a catalyst in the first instance [6]. From the accomplished temperature and composition measurements, information was derived about potential exhaust gas recirculation entraining into the fresh feed gas in the upflow cold wall reactor. Further, we applied Particle Image Velocimetry (PIV) to characterize the flow field arising close to the substrate surface also at CCVD operation conditions, so that we can knowingly select the process parameters that would be beneficial for the CNT deposition [7].

With the knowledge of the gas flow behavior and having proved the measurement technique for the *in situ* analysis of the gas phase, we have extended the Raman spectroscopy setup, so that we are now able to analyze both, the gas and solid phases *in situ* and simultaneously. The here reported approach enables the simultaneous *in situ* quantification of relevant physical variables in the gas phase, such as the gas temperature and the carbon source conversion as well as the monitoring of the solid phase with regard to the moment of CNT nucleation, time range of growth and catalyst deactivation but also quantitatively regarding the defect and disorder content in the growing CNTs considering the well-known D/G Raman ratio [8]. Two experiments implementing catalysts resulting from two different preparation methods were carried out in order to assess the catalyst performance.

2. Experimental details

2.1 Optically accessible cold wall reactor

The CNT deposition is carried out in a self-designed, vertically-oriented and optically accessible cold wall reactor, which is operated with an upflow configuration. The reactor had been originally designed to perform *in situ* Raman

investigations in the gas phase as it is reported elsewhere [6,7]. Now, in order to integrate an additional Raman spectroscopy setup for the *in situ* analysis of the solid phase, its design had to be modified with regard to an additional optical access and an alternative for gas feeding. Figure 1 shows a schematic cross-sectional drawing of the modified cold wall reactor. The main body is composed of a 250 mm-long stainless steel pipe with an internal diameter of 55 mm and a wall thickness of 5 mm. The reactor inner volume is about 600 cm^3. At both ends of the main body, two flanges are used to attach the reactor caps and O-rings assure closeness of the system.

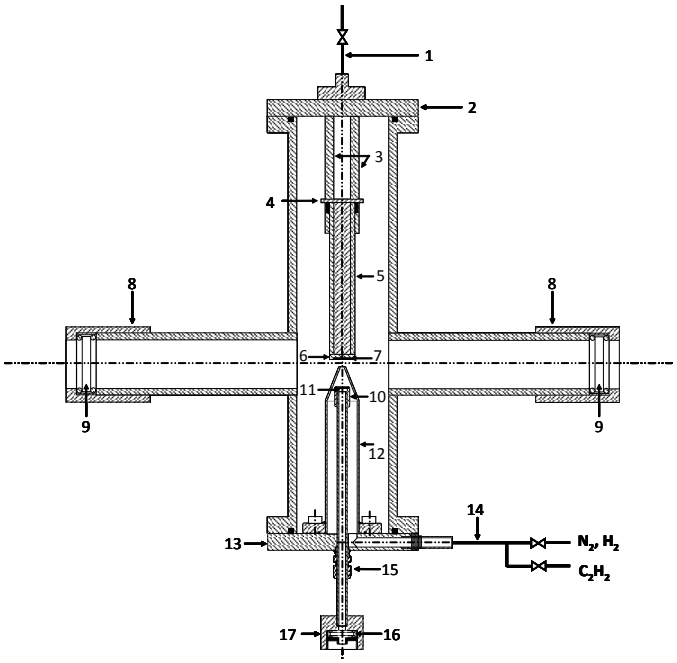

Fig.1. Schematic of the optically accessible cold wall reactor. 1: exhaust gas pipe, 2: reactor upper cap, 3: threaded rods, 4: heating support plate, 5: heating cartridge, 6: heating closure plate, 7: substrate wafer, 8: optical accesses for the gas phase analysis, 9: window for the gas phase analysis, 10: lens cap, 11: lens for the solid phase analysis, 12: nozzle for the feed gas, 13: reactor lower cap, 14: feed gas pipe, 15: nut for optical access attachment, 16: window for the solid phase analysis, 17: optical access for the solid phase analysis

For the *in situ* Raman monitoring of both phases, the reactor is equipped with several optical accesses. For the gas phase analysis, four optical accesses in form of tubes with an inner diameter of 29 mm are welded onto the main body in crosswise arrangement. Every tube is provided with an external screw thread at its end in order to mount a cylinder-shaped screw cap containing a removable window. For the solid phase analysis, an additional optical access is implemented at the bottom of the reactor. This access consists of an approximately 135 mm-long stainless steel pipe of 4 mm internal diameter and 1 mm wall thickness, of which its bottom end is welded onto a bushing. The bushing at the bottom end is used to hold a window, which is made of quartz glass Suprasil 1 (diam. = 14 mm, thickness = 2 mm) and two ring packings seal the window interface. On the top end of the access pipe a focusing and concurrently collecting lens for the solid phase analysis (see section 2.2) is placed and held by a lens cap. By means of a nut provided with back and front ferrules made out of perfluoroalkoxy (PFA), the optical access is attached to the reactor lower cap, enabling variation of its vertical position and thus, the position of the lens with respect to the substrate surface.

With the new reactor configuration, the fresh feed gas is introduced through an access located in the reactor lower cap and flows through a pipe (diam. = 22 mm), which is arranged concentrically to the optical access for the solid phase analysis and is provided with a nozzle of 4 mm internal diameter and 1 mm wall thickness at its end. After the

gas enters the reactor through the nozzle, it impinges the substrate surface and continues its way up to the outlet. By means of mass flow controllers (MFCs, Bronkhorst), the gas volumetric flow rate is regulated and controlled. The aspect ratio AR is defined as the ratio of the nozzle-to-substrate distance to the nozzle inner diameter and based on the results of previous experiments on the flow field [7], a constant value of AR = 1.25 has been selected. The upper inner part of the reactor mainly consisting of the heating cartridge construction, which is used to reach and keep the desired substrate temperature, remained unmodified as described elsewhere [7].

2.2 Raman spectroscopy setup

The entire *in situ* Raman spectroscopy concept consists of two independent setups for the analysis of the gas and solid phases. In order to couple both setups into the optical accesses available in the reactor, they have been aligned at different heights, so that the setup for the gas phase is adjusted 180 mm higher than the setup for the solid phase analysis. Fig. 2 shows a schematic of the entire measurement arrangement, where the CCVD reactor, the excitation and detection paths as well as the involved optical components and instrumentation can be seen.

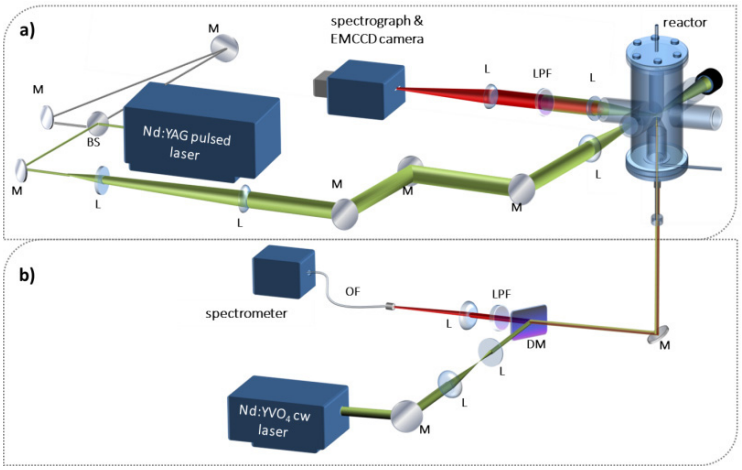

Fig. 2. Schematic of the Raman spectroscopy setup for *in situ* CCVD analysis. a) Raman setup for the gas phase analysis, b) Raman setup for the solid phase analysis. M: mirror, BS: beam splitter, L: lens, DM: dichroic mirror, LPF: long pass filter, OF: optical fiber.

The implemented Raman spectroscopy setup for the *in situ* gas phase analysis has been previously described in detail elsewhere [6] which will not be repeated here. For the *in situ* solid phase analysis a continuous wave diode-pumped Nd:YVO_4 laser, emitting light at a wavelength of 532 nm with a power of 250 mW, is used for the excitation of the solid phase. After passing a lambda-half wave plate, the laser beam enters a telescope, which is constituted of two spherical lenses (f = 100 mm and f = 50 mm), in order to collimate and contract the laser beam diameter by half. A beam splitter, which is highly transmissive for wavelengths longer than 545 nm and highly reflective for the excitation wavelength, directs the laser beam to a 45°-mirror, which is located underneath the reactor and which is highly reflective (99%) for wavelengths in the range of 400-750 nm . Further, the laser beam is brought into the optical access and reaches a spherical lens (diam. = 6.5 mm, f = 18.4 mm), which focuses it onto the substrate surface. In order to exactly adjust its focal length onto the substrate surface, a linear translation stage has been attached to the optical access pipe so that the optical access and consequently, the position of the lens can be vertically shifted. The Raman spectroscopy setup for the *in situ* solid phase analysis is arranged in backscattering direction, i.e. the scattered light is collected by the same focusing lens (f = 18.4 mm) at 180° with respect to the laser excitation direction. Thus, the elastically and inelastically scattered light is guided all the way back through the optical access to the 45°-mirror and then to the beam splitter. By means of the beam splitter and a long pass filter (highly transmissive for wavelengths longer than 539 nm), the interfering strong elastically scattered light is removed. Further, the inelastically scattered light is focused by an achromatic doublet (f = 100 mm) onto the entrance of a round-to-linear fiber bundle, which guides the Raman signals to a spectrometer (QE65 Pro, Ocean

Optics) provided with a back-illuminated CCD sensor (1024 x 58 pixels). The exposure time for the acquisition of a single spectrum has been max. 2 s and the given spectral resolution is 5.6 cm^{-1}.

In order to additionally perform post-CCVD Raman measurements on the substrates, an *ex situ* Raman spectroscopy setup is integrated into the *in situ* arrangement. By inserting the indicated removable mirror for *ex situ* Raman, the laser beam is restrained to enter the reactor but is reflected at 45° in the same optical plane and reaches a spherical lens (diam. = 6.5 mm, f = 18.4 mm), which is identical to the one located inside the reactor. By means of this lens, the laser beam is focused onto the substrate, which is attached onto a two directional translation stage to facilitate the measurement at different spots on the substrate surface. By conducting *ex situ* Raman measurements on the substrate wafers, it is possible to validate the measurements carried out *in situ* with regard to representativeness and accuracy of the estimated D/G ratio

2.3 Experimental procedure

In the CCVD process, the fresh feed flow is composed of nitrogen, hydrogen and acetylene with a defined composition. Nitrogen. with a purity of more than 99.999 %, serves as carrier gas since it is not involved in the gaseous chemical reaction and it conforms the major fraction of the total feed flow rate. Hydrogen shows a purity of more than 99.999 % and is used as a supporting reductive gas to improve catalyst utilization for CNT formation avoiding the deposition of amorphous carbon. Acetylene, which is the carbon feedstock, is available with a purity of more than 99.5 %. Silicon wafers are used as catalyst substrates and are provided with diverse support layers, e.g. Al_2O_3 or SiO_2. For the preparation of the Fe_2O_3 catalyst nanoparticles, two different methods are applied, namely spin coating and metal organic chemical vapor deposition (MOCVD). After catalyst preparation, the substrates provided with the corresponding catalysts are transferred to the CCVD reactor and during the heating-up process for reaching the CCVD operation temperature ($T_{substrate}$ = 953 K), N_2 and H_2 are fed in a 3:1 volumetric ratio to reduce the Fe_2O_3 catalyst to elemental Fe.

Two CCVD experiments, designated as I (spin coating) and II (MOCVD), have been carried out applying *in situ* Raman monitoring of the solid and gas phases.

3. Results and discussion

3.1 In situ Raman monitoring of the solid phase

The Raman features arising from the photophysical and mostly resonant scattering process in nanocarbon materials, e.g., graphite, graphene, amorphous carbon, CNTs and CNFs, are well known [9]. Particularly relevant for the here reported studies are the so-called D and G bands, with Raman shifts located at approximately 1330 cm^{-1} and 1590 cm^{-1}, respectively. The first-order-allowed G band involves the in-plane bond stretching motion of pairs of C sp^2 atoms at all sites, so that this mode does not require the presence of sixfold rings. The double-resonant D band is a breathing mode, which is forbidden in perfect graphite and only becomes active in the presence of defects and disorder; it is dispersive and its intensity is strictly connected to the presence of sixfold aromatic rings [10]. Thus, by monitoring the appearance and development of the characteristic D and G Raman bands, we are able to trace *in situ* the formation and growth processes of nanocarbon materials. As mentioned before, the emergent solid phase is monitored within a centrally-located spot of approximately 3 μm in diameter, so that the acquired Raman signals are the result of the contribution of all nanocarbons grown in the spot. Thus, a distinction between CNTs, CNFs and amorphous carbon cannot be established on the basis of the *in situ* Raman spectra, so that post-CCVD SEM analysis is necessary to find out, which carbon nanostructures have been grown in the *in situ* measurement location. For this reason, we refer the emerging solid phase to as nanocarbons and not as CNTs in the first instance.

Analyzing first the raw spectra , it can be noticed that during the first six minutes after the onset of the reaction, i.e. after acetylene addition to the feed flow, the Raman spectra only exhibit the SiO_2 peak but no D and G bands are observable. This indicates either that any nanocarbons are formed yet or that the SNR is still too low to identify the D and G bands out of the noise level. Considering now the spectrum acquired at t = 7 min, first changes in the spectral region of interest are observed, corresponding to the moment when the Raman signals of nanocarbon

formation are first detectable. In the further course, the Raman signal intensities of the D and G bands increase considerably until t = 15 min, indicating the time for growth or for the formation of more nanocarbons. After the fifteenth minute, any changes in both peak intensities cannot be observed. Thus, in a qualitative manner, it can be stated that the nanocarbon formation in experiment I starts not before the sixth minute after acetylene addition. Thereafter, the carbon nanostructures grow or more nanocarbons are formed, as it is noticeable from the intensity increase of the D and G bands until the 15th minute and subsequently, it slows down and stops until no further change is observable. Hence, merely on the basis of the raw data it is already possible to draw significant conclusions about what happened inside the CCVD reactor with regard to the moment of nanocarbon formation, growth and catalyst deactivation.

Considering now the raw Raman spectra, it is possible to monitor once more the temporal evolution of the D and G bands and accordingly, the formation and growth of the emergent carbon nanostructures. Contrary to what has been observed in experiment I, here a rather rapid catalyst activity is noticed as already at short times after acetylene addition, first spectral changes are found. At t = 30 s, the characteristic D and G bands are visible for the first time. Subsequently, more nanocarbon formation and growth proceed considerably according to the increase of both D and G band intensities. However, after one minute yet the intensity increase ceases, so that the deposition might be potentially completed as a result of a rapid catalyst deactivation.

Thus, based on the raw spectra acquired *in situ* out of the emerging solid phase in both experiments, it is also possible to gain information about the catalyst performance. The catalyst prepared by MOCVD (experiment II) shows hereby a faster catalytic activity, which is reflected in the rapid formation process but also in the rapid catalyst deactivation, probably due to catalyst covering with amorphous carbon. Contrary to this behavior, the catalyst prepared via spin coating (experiment I) exhibits a rather long delay time to initiate the nanocarbon formation and since longer growth times are observed, a longer catalytic activity is on hand. Not only qualitative insight can be gained from the *in situ* Raman spectra, but also quantitative information on the basis of the D/G ratio, which is frequently used as a reliable parameter to assess the degree of disorder and defect content in carbon materials. As the D band is associated with the presence of defects and disorder, the lower the D/G ratio, the better the structural quality of the carbon material. Since the shapes and line widths of the D and G Raman bands are known to be strongly affected by several factors, like clustering of the sp^2 phase, bond disorder, presence of sp^2 rings or chains [10], it should be clarified whether the ratio of the peak heights I_D/I_G or the ratio of the peak integrals A_D/A_G is the most adequate to assess the quality of the carbon nanostructures of experiments I and II.

The normalization to the respective G band maxima enables a clear visualization of the shapes of both bands as well as the D peak heights. Since the Raman bands show some degree of overlapping in both spectra (I and II), the resulting multiple fitted peaks with their corresponding heights and FWHMs are indicated. When comparing the peak shapes first, it can be noticed that in experiment II comparatively narrow line widths of both bands are on hand and therefore, the degree of overlapping of the D and G bands is less. In experiment I in contrast, the G and especially the D band exhibit a large line width and thus, overlap to a higher extent. The D bands feature different peak heights: for experiment II, the D peak height is larger than G and for experiment I, lower. In the following we report both I_D/I_G and A_D/A_G ratios for comparison.

When analyzing the temporal progress of both I_D/I_G and A_D/A_G ratios, no clear changes in the structural quality of the growing carbon nanostructures but a rather constant D/G level was observed. The nanocarbons grow between the seventh and the fifteenth minute after acetylene addition, however, their disorder and defects content remain invariant in this period of time. This means that once the nanocarbons form, they essentially grow without changing their original structural quality or more nanocarbons are formed with similar disorder and defect content until the catalyst is deactivated. Since both I_D/I_G and A_D/A_G ratios do not significantly change over the regarded reaction time (t = 8 – 30 min), their mean values have been estimated to $I_D/I_G = 1.054 \pm 0.011$ and $A_D/A_G = 2.205 \pm 0.088$, as listed in Table 1. The disparity in the resulting D/G ratios shows why it is important to select the most appropriate D/G ratio for the structural quality assessment of the growing nanocarbons. By looking at the temporal progress of the D and G peak heights and integrals , it can be noticed that the peak heights of both bands develop equally during the entire regarded reaction time leading to $I_D/I_G \sim 1$. The peak integrals, on the contrary, develop differently, so that the D peak features an area approximately twice that one of the G peak, leading to $A_D/A_G \sim 2$. Thus, if $I_D/I_G \sim 1$ and $A_D/A_G \sim 2$, then the D line width should be twice that one of the G band (as it is reported in Table 1) and thus, should be exclusively the reason of the disparity between the estimated I_D/I_G and A_D/A_G ratios.

Additionally to the *in situ* Raman results in the solid phase of experiment I, the substrate wafer has been analyzed *ex situ* via Raman spectroscopy in sixteen different measurement points within an area of 4 mm^2 located in the central region of the wafer. The estimated *ex situ* mean values of the I_D/I_G and A_D/A_G ratios and their corresponding standard deviations are indicated in Table 1.

Table 1. Results on the solid phase quantitative analysis of experiments I and II.

Exp.		*I_D/I_G ratio*	*FWHM-D / cm^{-1}*	*FWHM-G / cm^{-1}*	*A_D/A_G ratio*
I	*in situ*	*1.054 ± 0.011*	*263.344 ± 5.603*	*126.861 ± 3.676*	*2.205 ± 0.088*
	ex situ	*0.949 ± 0.007*	*231.244 ± 5.852*	*126.800 ± 3.331*	*1.819 ± 0.044*
II	*in situ*	*1.459 ± 0.037*	*105.996 ± 2.388*	*74.125 ± 1.969*	*2.083 ± 0.082*
	ex situ	*1.329 ± 0.019*	*103.248 ± 1.917*	*72.700 ± 1.357*	*1.795 ± 0.063*

First, the low standard deviations of the D/G ratios estimated *ex situ* suggest that carbon nanostructures with rather similar structural quality have been likely grown over larger areas on the substrate, when compared with the *in situ* measurement spot of 3 μm in diameter. Thus, this shows that the *in situ* monitoring of the nanocarbon formation carried out at a single point on the substrate in experiment I is certainly representative for larger areas within the central region of the substrate. Further, when considering the absolute values of the D/G ratios, it can be noticed that a good correlation between the I_D/I_G ratios estimated *in situ* and *ex situ* exists, which is an indication for the reliability of both the practical implementation of the *in situ* Raman spectroscopy setup and the numerical approach for spectra evaluation. However, the *ex situ* A_D/A_G ratio exhibits a significant lower value than the *in situ* A_D/A_G ratio. This can be explained by analyzing the corresponding band line widths listed in Table 1, which both have been estimated to be larger *in situ* than those measured *ex situ*, especially in the case of FWHM-D.

Consequently, both I_D/I_G and A_D/A_G ratios in experiment II are larger than one, whereby $A_D/A_G > I_D/I_G$, which essentially matches the disparity trend observed also in experiment I. However, when comparing the estimated D/G values of both experiments, contradicting assessments arise as $(I_D/I_G)_I < (I_D/I_G)_{II}$ and $(A_D/A_G)_{II} < (A_D/A_G)_I$. This means that when considering the I_D/I_G ratio, experiment I will appear to deliver higher structured nanocarbons (due to the lower D/G ratio) than experiment II and when considering the A_D/A_G ratio, the assessment would be exactly the opposite. This indicates once again the importance of selecting the proper D/G ratio to assess the defect and disorder content of the growing nanocarbons. In order to explain the contradicting outcome regarding the D/G ratios, it is first clear that $(I_D/I_G)_I < (I_D/I_G)_{II}$ because $I_D \approx I_G$ in experiment I whereas $I_D > I_G$ in experiment II. Further, to clarify why $(A_D/A_G)_{II} < (A_D/A_G)_I$, it is important to consider the band line widths available in both experiments. The mean line widths of the D and G bands of experiment II have been estimated and reported in Table 1 to be significantly narrower than those of experiment I, whereby the FWHM-D is broader than FWHM-G as it is the case in experiment I but to a lesser extent, so that $(\text{FWHM-D/FWHM-G})_{II} < (\text{FWHM-D/FWHM-G})_I$. Thus, this information on the FWHMs explains both the comparatively lower peak integrals and lower A_D/A_G ratios estimated for experiment II.

By means of *ex situ* Raman characterization, mean values of the I_D/I_G and A_D/A_G ratios as well as their corresponding standard deviations have been estimated from at least sixteen measurement points and the results are indicated in Table 1. Regarding first the estimated standard deviations, it can be noticed that they are larger compared to those of experiment I, but still low to suggest that carbon nanostructures with rather similar structural quality over larger areas on the substrate have been likely grown. Similarly to the results of experiment I, a strong correlation between the absolute values of the I_D/I_G ratios estimated *in situ* and *ex situ* is noticeable whereas an underestimation for the *ex situ* A_D/A_G ratio is on hand.

In order to find out what kind of nanostructures have been in fact grown, *ex situ* characterization of the deposited nanocarbons via SEM in the central region of the substrates has been performed. Fig. 3a - c show the *ex situ* SEM images from the resulting nanocarbons of experiment I. In the first instance, it can be noticed that the probed area is covered with CNT-like, cross-linked insular structures and no other kind of carbon materials, like amorphous carbon,

have been deposited (Fig. 3a). The tubes seem not to have grown aligned over the whole substrate surface but distorted, nesting in sort of catalyst islands and spreading laterally along the substrate; therefore, some empty spaces are seen on the wafer (Fig. 3b). The CNTs, which have been deposited during experiment I, feature diameters in the range of about 15 nm (Fig. 3c). The SEM images depicted in Fig. 3d - f show the type of carbon material deposited in experiment II. The major part of the examined area is covered with comparatively more deposited material, consisting mainly of amorphous carbon and tube or fiber-like structures with different dimensions (see 3d). In some locations, mainly amorphous carbon and only a few short tube-like structures have been deposited (see Fig. 3e). The detected tube-like structures exhibit strong diverging diameters in the range of 50 – 160 nm (3e and f).

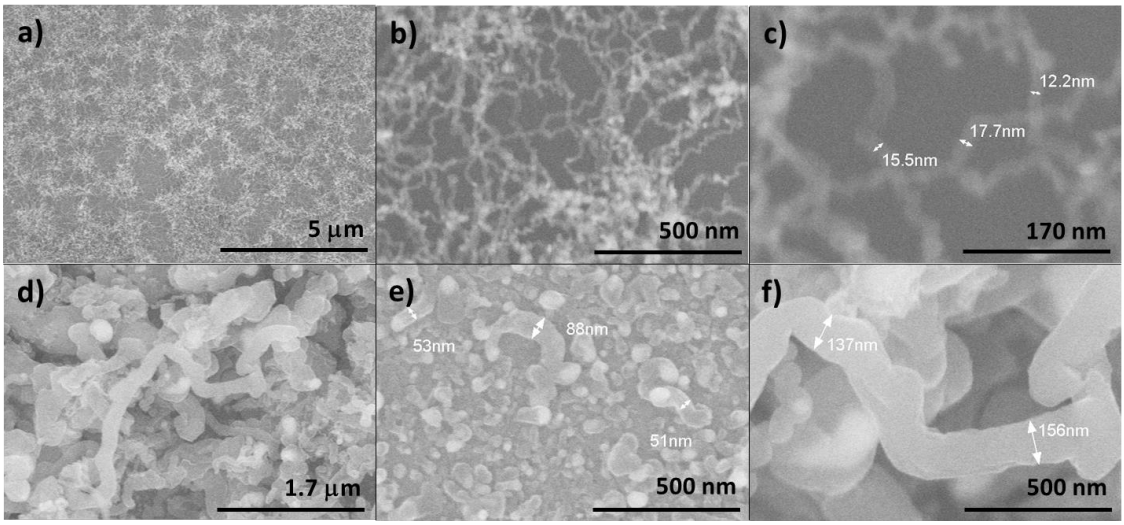

Fig. 3. *Ex situ* SEM analysis of the resulting carbon structures from experiment I (a, b and c) and experiment II (d, e and f).

By first analyzing the structural quality of the growing or grown nanocarbons, the *in situ* as well as the *ex situ* estimated I_D/I_G ratios suggest that the degree of disorder and defect content of the carbon nanostructures grown in experiment I is less than those formed in experiment II. When establishing a correlation between the Raman results with the corresponding SEM images, it is possible to further understand why rather large I_D/I_G ratios have been obtained for both experiments. From the SEM images of experiment I, better I_D/I_G ratios would be likely expected, since any amorphous carbon, which could contribute worsening the monitored quality ratio, is present in the region of interest. Instead, tube-like nanostructures with relatively small diameters have grown but distorted, spreading laterally along the substrate surface and exhibiting tube bending on their surface, which might be the reason of the rather large estimated I_D/I_G ratio. In contrast, the SEM images of experiment II reveal the deposition of mainly amorphous carbon and only a few tube-like structures, whereby the presence of amorphous structures is in fact reflected in the higher estimated I_D/I_G ratio.

3.2 In situ Raman monitoring of the gas phase

Simultaneously to the *in situ* measurements of the emergent solid phase, the gas phase of experiments I and II was also monitored by applying Raman spectroscopy. Figure 4 shows the temporal progress of the gas temperature and the acetylene conversion fraction X_{C2H2} during experiments I and II. The progress of the two monitored variables is only shown for the time period t = 1 – 10 min, as later gas temperature and X_{C2H2} for both experiments exhibit a rather constant course. In order to better assess the gas parameters of experiments I and II, additional experiments were carried out and monitored at the same CCVD operation conditions and measurement locations as I and II, but without the use of any catalyst. The resulting mean values and standard deviations are integrated in Fig.4

for comparison.

Regarding first the temporal progress of the gas temperature, no significant fluctuations at the time instants of CNT formation for the respective experiments (t_I = 6 min and t_{II} = 0.5 min) nor over the entire regarded time period can be observed but a rather relatively even course. Thus, by calculating the average gas temperature, temperature levels of T_I = 956 ± 16 K and T_{II} = 973 ± 19 K are attained for experiments I and II, respectively. For comparison, the average gas temperature values for the experiments conducted without any catalyst are $T_{A\text{-without\_cat}}$ = 959 ± 30 K and $T_{B\text{-without\_cat}}$ = 1060 ± 68 K. As it can be noticed, all gas temperatures measured with and without catalyst are higher than the wafer temperature $T_{substrate}$ = 953 K. This is attributed to the exothermic decomposition of acetylene in the gas phase, which is measurable at the respective measurement locations in the vicinity of the substrate surface

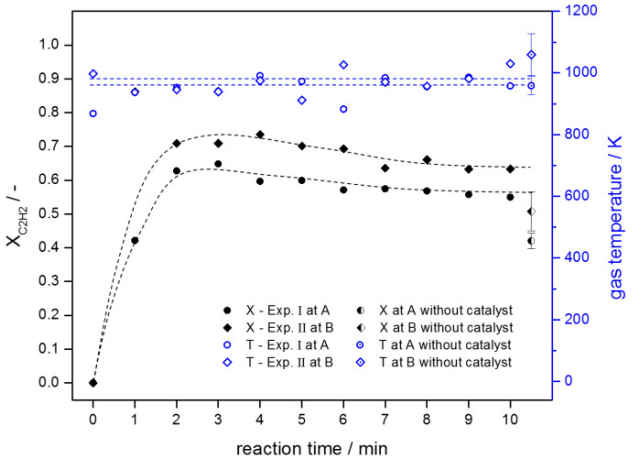

Fig. 4. Temporal progress of the conversion fraction X_{C2H2} and the gas temperature of experiments I and II. Additional mean values and standard deviations of the gas parameters are provided from experiments without the use of a catalyst but at the same operation conditions and measurement locations as I and II.

However, when applying a catalyst, as in experiments I and II, different thermal processes arise additionally. Since the adsorption of the carbon source, carbon diffusion through the catalyst bulk or over the catalyst surface and the precipitation of elemental carbon are reported to be endothermic processes [5], a gas temperature reduction close to the substrate is expected in case that the endothermic processes prevail over the exothermic decomposition of the carbon source. This is confirmed by the rather slow catalyst performance observed during *in situ* Raman monitoring of the solid phase and by the resulting low carbon yield determined by the SEM images shown in Fig. 3a – c, where comparatively few carbon structures were deposited. With respect to the gas temperatures measured at location B, we find that $T_{II} < T_{B\text{-without\_cat}}$, which means that in this case, the endothermic processes taking place in the presence of the implemented catalyst in experiment II prevail over the exothermic acetylene decomposition, thereby inducing a gas temperature reduction. In principle, a constant temporal progress of the gas temperature at the respective measurement locations close to the substrate is an indication that no greater recirculation of the participating gases with coincidental vortex generation occurs within the flow field and therefore, a likely uniform CNT growth is favored. However, in the outer region of the reactor, temperature and consequential density gradients may arise because of the colder reactor wall, possibly influencing the gas temperature at measurement location B. To analyze the *in situ* monitored acetylene conversion fraction, it is important to clarify first its meaning on the basis of the gas phase Raman spectra, as by monitoring the gas flow composition during experiments I and II and during the experiments carried out without applying any catalyst, X_{C2H2} is ultimately accessible. Thus, the estimated carbon source conversion involves the C-C bond dissociation of the fed acetylene molecules either for gas pyrolysis, formation of other minor gaseous compounds or in fact, for carbon-catalyst dissolution to form solid carbon structures. By looking now at the temporal progress of X_{C2H2} during experiments I and II , it can be noticed that right

after feeding acetylene at t = 0 min, the X_{C2H2} curve progress exhibits a steep increase due to the slow stabilization of the adjusted acetylene volumetric flow rate (0.85 SCCM). Afterwards, a slight reduction of the conversion fraction is observable until it reaches a steady level at $X_{C2H2\text{-}I} = 0.55$ and $X_{C2H2\text{-}II} = 0.65$ for experiments I and II, respectively. For comparison, the attained rather constant conversion levels of the experiments conducted without any catalyst are $X_{C2H2\text{-}A\text{-}without\_cat} = 0.42 \pm 0.02$ and $X_{C2H2\text{-}B\text{-}without\_cat} = 0.51 \pm 0.06$ at locations A and B, respectively. Similar to what has been observed in the gas temperature progress, we find that $X_{C2H2\text{-}B} > X_{C2H2\text{-}A}$, with and without applying a catalyst. In the case where no catalyst was used, this may be attributed exclusively to the fact that the rate constant of the thermal decomposition of acetylene is known to be a function of temperature and can be described with an Arrhenius approach. In the case of experiments I and II, the additional effect of the implemented catalysts on the acetylene conversion fraction has to be taken into account. When comparing first the acetylene conversion fractions measured at location A, we find that when applying the catalyst prepared via the spin coating method, approximately 13% more acetylene is converted or dissociated than in the case where no catalyst is used. Regarding now the conversion fractions monitored in location B, a slightly higher acetylene conversion difference of 14% is observed when comparing X_{C2H2} of experiment II with X_{C2H2} of the experiment conducted without any catalyst. By correlating this information with the gas temperature T_{II} and the insights attained from the *in situ* and *ex situ* characterization of the solid phase, it can be inferred that due to the higher catalytic activity, it is likely that the dissociated C atoms are employed for the formation of solid carbon nanostructures instead of recombining in the gas phase.

4. Conclusions

The present paper reports on the first results of the successful application of an *in situ* measurement technique based on linear Raman spectroscopy, which has been established to simultaneously monitor the parameters of interest in the solid and gas phases during CNT formation and growth in a cold wall reactor via CCVD. Thus, it is possible to assess the catalytic activity departing from both *in situ* solid and gas phase parameters, offering therewith new possibilities for process fundamental research and process optimization towards a CNT-tailored production

Acknowledgements

The authors gratefully acknowledge financial support for parts of this work by the German Research Foundation (DFG), which additionally funds the Erlangen Graduate School in Advanced Optical Technologies (SAOT) in the framework of the German excellence initiative. Additionally, we would like to thank Alexander Lodermeyer for developing the spectra evaluation routine.

References

[1] C. Singh, M. S. P. Shaffer, and A. H. Windle, Production of controlled architectures of aligned carbon nanotubes by an injection chemical vapour deposition method, Carbon 41 (2003) 359-368.
[2] S. Hofmann, R. Blume, C. T. Wirth et al., State of Transition Metal Catalysts During Carbon Nanotube Growth, The Journal of Physical Chemistry C 113 (2009) 1648-1656.
[3] J. Y. Raty, F. Gygi, and G. Galli, Growth of carbon nanotubes on metal nanoparticles: A microscopic mechanism from ab initio molecular dynamics simulations, Physical Review Letters 95 (2005).
[4] S. McCaldin, M. Bououdina, D. M. Grant, and G. S. Walker, The effect of processing conditions on carbon nanostructures formed on an iron-based catalyst, Carbon 44 (2006) 2273-2280.
[5] S. Esconjauregui, C. M. Whelan, and K. Maex, The reasons why metals catalyze the nucleation and growth of carbon nanotubes and other carbon nanomorphologies, Carbon 47 (2009) 659-669.
[6]. K. Reinhold-López, A. Braeuer, N. Popovska, and A. Leipertz, In situ monitoring of the acetylene decomposition and gas temperature at reaction conditions for the deposition of carbon nanotubes using linear Raman scattering, Optics Express 18 (2010) 18223-18228.
[7] K. Reinhold-López, A. Braeuer, A. Schmitt, N. Popovska-Leipertz, and A. Leipertz, Flow field characterization in a vertically oriented cold wall CCVD reactor by particle image velocimetry, Chemical Engineering Journal 184

(2012) 315-325.
[8] M. S. Dresselhaus, G. Dresselhaus, R. Saito, and A. Jorio, Raman Spectroscopy of Carbon Nanotubes, Physics reports 409 (2005) 47-99.
[9] A. C. Eckbreth, Laser Diagnostics for Combustion Temperature and Species, 1988.
[10] G. Brouwer, and J. A. J. Jansen, Deconvolution method for identification of peaks in digitized spectra, Analytical Chemistry 45 (1973) 2239-2247.